Materials Today Advances 12 (2021) 100180

Contents lists available at ScienceDirect

Materials Today Advances

journal homepage: www.journals.elsevier.com/materials-today-advances/

A Resonance Raman spectroscopic study on charge transfer enhancement in photosensitizers

Wang-Hyo Kim [a, b, 1], Joseph I. Mapley [c, 1], Deok-Ho Roh [a, b, 1], Jeong Soo Kim [a, b], So Yeon Yoon [a, b], Keith C. Gordon [c, **], Tae-Hyuk Kwon [a, b, *]

[a] Department of Chemistry, Ulsan National Institute of Science and Technology (UNIST), Ulsan, 44919, Republic of Korea
[b] Center for Wave Energy Materials, UNIST, Ulsan, 44919, Republic of Korea
[c] Department of Chemistry, University of Otago, PO Box 56, Dunedin, New Zealand

ARTICLE INFO

Article history:
Received 10 August 2021
Received in revised form
13 October 2021
Accepted 14 October 2021
Available online xxx

Keywords:
Photosensitizer
Charge transfer property
Quinoidal property
Resonance Raman spectroscopy
Density functional theory calculation

ABSTRACT

The charge transfer (CT) properties of photosensitizers largely determine the photovoltaic performances of dye sensitized solar cells (DSSCs). Thus, understanding the CT properties of photosensitizers is key to further improving the performances of DSSCs. We herein investigated the underlying relationship between the molecular structures and CT properties of the photosensitizers using resonance Raman (RR) spectroscopy and density functional theory (DFT) calculations. RR spectroscopy combined with DFT calculations showed that the presence of a triple bond (**T-D1**, **T-D2**, and **T-D3**) enhanced the degree of CT from the donor to the acceptor. In addition, the presence of electron donating groups (EDGs) on the donor (**T-D2** and **T-D3**) further increased the CT properties of the donor. Moreover, DFT analysis based on the harmonic oscillator model of aromaticity revealed that the presence of a triple bond and an EDG increased the quinoidal character of the photosensitizer in the excited state. Finally, it was found that the degree of CT properties exhibited by each photosensitizer was in good agreement with the order of the DSSC performances.

1. Introduction

Dye-sensitized solar cells (DSSCs) based on thin films have been investigated for use as promising indoor power generating photovoltaic cells owing to their fast charge transport properties, retarded charge recombination, and high efficiency under dim light [1–4]. These properties render DSSCs potentially suitable for applications in building-integrated photovoltaics and wireless power generators for small electronics [5]. To accelerate the commercialization of DSSCs, many researchers have investigated the enhancement of the power conversion efficiencies (PCEs) of DSSCs through the use of thin TiO_2 films ($\lesssim$3.5 μm) [6,7]. Consequently, the relationships between the electronic dynamics and the DSSC performances of such systems have been reported [8,9]. Typically, the charge injection efficiency, which depends on the charge transfer (CT) property of a photosensitizer, has been reported to dominantly determine the performances of DSSCs possessing thin film photoanodes [10]. In addition, the CT properties of the photosensitizers are largely dependent on their molecular structures, and therefore, it is crucial to understand the relationship between the molecular structure and the CT properties to improve the performances of DSSCs.

To enhance the CT properties, a general photosensitizer structure has been developed based on electron donor–π-bridge–electron acceptor (D–π–A) structures [11–14]. As a result, one of the highest performances reported to date was presented, wherein a PCE of 13.0% was achieved using a porphyrin-based sensitizer, **SM315**, which contained an ethynyl (triple) bond and a benzo[*c*][1,2,5]thiadiazole (BTD) spacer between the donor and acceptor groups [14]. **SM315** exhibited an increased absorption range and a

* Corresponding author.
** Corresponding author.
E-mail addresses: keith.gordon@otago.ac.nz (K.C. Gordon), kwon90@unist.ac.kr (T.-H. Kwon).
[1] W.-H.K., J.I.M. and D.-H.R. contributed equally to this work.

https://doi.org/10.1016/j.mtadv.2021.100180

superior incident photon-to-electron conversion efficiency (IPCE) due to the quinoidal property of the triple bond and the BTD unit [15,16]. To further investigate the effect of the triple bond and the quinoidal property, we previously modified dithieno[3,2-*b*:2′,3′-*d*] thiophene (DTT)-based photosensitizers with different bond types between the donor and the π-bridge (**S-D1** for single, **D-D1** for double, and **T-D1** for triple bonds) and bearing an electron donating group (EDG) at the *para* position of the donor (**T-D2** for methoxy-, and **T-D3** for N-carbazolyl EDGs) (Fig. 1a). It was found that the triple bond-incorporated photosensitizer (**T-D1**) exhibited a higher charge injection efficiency compared to the corresponding structures containing single (**S-D1**) or double bonds (**D-D1**) [17]. Furthermore, the photosensitizer containing an EDG (**T-D2**) exhibited an increased photocurrent density that was correlated to the donating ability of the EDG [18]. However, these previous works and other molecular engineering studies focused on the effects of structural modification of the photosensitizers in terms of charge recombination, regeneration, and injection in the DSSCs [19–25], with no spectroscopic evidence being available regarding the CT nature and quinoidal properties of the photosensitizers.

Thus, we herein report a spectroscopic and computational study on the CT and quinoidal properties of five DTT-based photosensitizers (**S-D1**, **D-D1**, **T-D1**, **T-D2**, and **T-D3**) using resonance Raman (RR) spectroscopy and density functional theory (DFT) calculations. RR spectroscopy was selected due to its ability to reveal vibrational modes that mimic changes in the charge density as a result of specific electronic transitions probed with different excitation wavelengths (Fig. 1b) [26]. More specifically, RR spectroscopy excites molecules of interest to electronic excited states (E_1 and E_2), which correspond to intramolecular charge transfer (ICT) and $\pi-\pi^*$ transitions. Non-resonant Raman spectroscopy (Fig. 1b(i)) acts as a reference, where molecules are excited from the electronic ground state (E_0) to the virtual state [27–29]. Thus, the RR spectra shown in Fig. 1b(ii) and 1b(iii) can indicate the vibration modes involved in the corresponding electronic transitions, consequently allowing elucidation of the molecular structure that contributes to the enhanced CT properties. Hence, the effect of the bond type and the EDGs on the nature of the electronic transitions can be observed through changes in the vibrational modes that are enhanced in the RR spectra. These spectroscopic changes correspond to the quinoidal properties confirmed by DFT calculations in terms of changes in the bond lengths and quinoidal character (Q) based on the harmonic oscillator model of aromaticity (HOMA) analysis. Based on spectroscopic and computational investigations, we aim to unveil the relationship between the molecular structures and CT natures of photosensitizers. In addition, the effects of structural modification on the photocurrent density are examined by evaluation of the device performance of a DSSC containing a thin photoanode (3.5 μm). This study will therefore be expected to deliver new insights into molecular engineering strategies for enhancing the CT and quinoidal properties of photosensitizers.

2. Experimental section

2.1. Materials

All chemicals and reagents were purchased from Aldrich, Alfa Aesar, TCI, and Acros and used without further purification. Reactions were performed using anhydrous solvent prepared by molecular sieves prior to use under inert atmosphere of nitrogen or argon. Silica gel was used for flash column chromatography, and thin layer chromatography was performed on silica gel glass (0.2 mm thick). All syntheses of the photosensitizers were carried out as previously reported [17,18,30] and ^{1}H and ^{13}C nuclear magnetic resonance spectroscopy (NMR) spectra of the photosensitizers are presented in the Supplementary Data (Part 8).

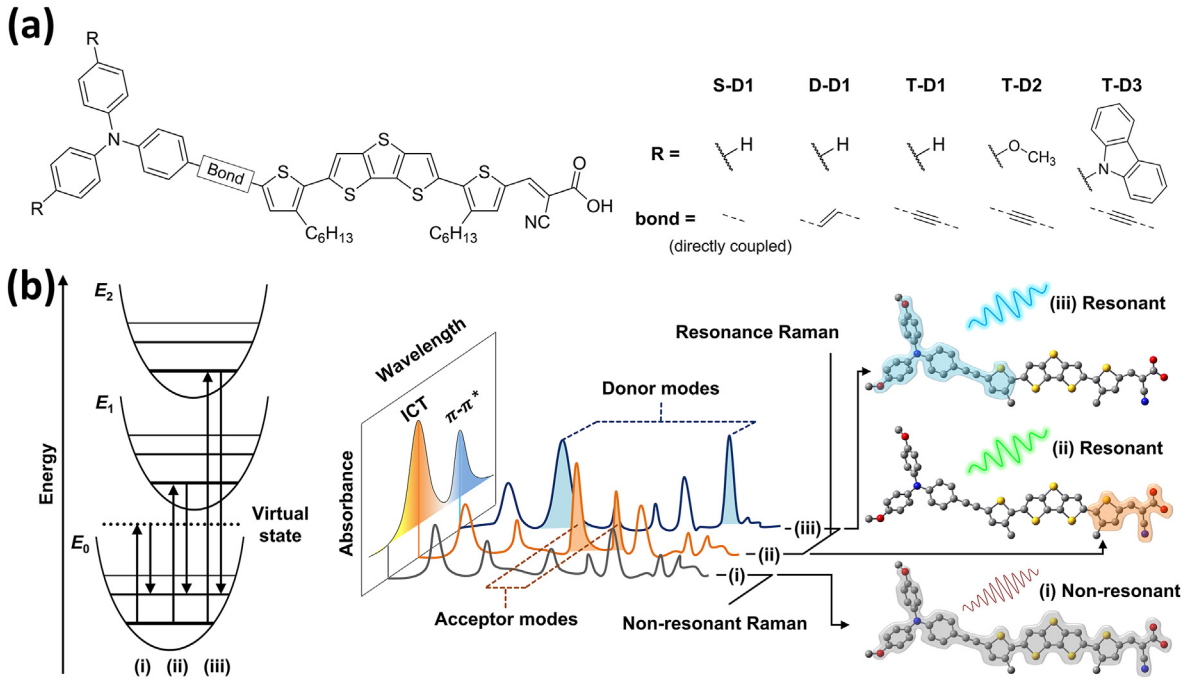

Fig. 1. (a) Molecular structures of the DTT-based photosensitizers. (b) Schematic illustration of resonance Raman (RR) spectroscopy. The energy level diagram shows the states involved in non-resonant and resonance Raman spectroscopy (left). The RR spectra exhibit an enhanced Raman intensity compared to the non-resonant Raman spectrum (middle). Thus, the vibrational mode involved in the RR spectra contributes to charge transfer (right).

2.2. Computational details

Geometry optimizations and vibrational calculations were performed using density functional theory (DFT) calculations with B3LYP [31,32] or CAM-B3LYP [33] functionals. Both functionals employed the basis set 6-31G(d) and were conducted with and without a solvent field implemented using a polarized continuum model [34]. These were implemented with Gaussian 09 D0.1 (Gaussian Inc, Wallingford, CT, USA) [35]. Scaling factors of 0.975 and 0.95 for B3LYP and CAM-B3LYP, respectively, were applied to calculated vibrational frequencies as recommended previously [36]. The vibrational modes were visualized using Molden [37].

Time-dependent DFT (TD-DFT) methods were implemented on the optimized structures, using both B3LYP and CAM-B3LYP hybrid functionals to approximate electronic transition energies and oscillator strengths for each photosensitizer investigated. Molecular models for calculations have alkyl chains shortened to a methyl group to simplify the calculation processes.

2.3. Spectroscopic methods

Spectroscopic grade solvents were used for all spectroscopic measurements. Spectral data was analyzed and manipulated using GRAMS v9.2 (Thermo Fisher Scientific) and OriginPro v9.0 (OriginLab Corporation). UV−vis absorption spectra of 2×10^{-5} M solution in dichloromethane (DCM) were recorded on a UV-2600 spectrophotometer (Shimadzu Corporation, Japan), and a FS5 fluorometer (Edinburgh Instruments, UK), with a Xenon Arc lamp light source.

FT Raman spectra were obtained with solid KBr-based pellet samples of the photosensitizers using a MultiRAM spectrometer (Bruker Optics, Ettlingen, Germany) and a liquid-nitrogen-cooled Model D418T germanium detector. The system was controlled by Bruker Opus v7.5 software. A 1064 nm Nd:YAG laser was used with a power of 150 mW. Spectra were measured with a spectral resolution of 4 cm^{-1} and 1024 scans.

Resonance Raman spectra were collected using a setup described previously [38]. In summary, the laser beam was focused on a spinning NMR tube in a 135° backscattering geometry with a 50 μm entrance slit. An Innova I-302 krypton ion laser (Coherent Inc., Santa Clara, CA, USA) was used to provide excitation wavelengths of 406 and 413 nm. Solid state diodes provided excitations wavelengths of 458, 515 (Cobolt, Solna, Sweden), 375 and 448 nm (CrystaLaser, Reno, NV, USA). Notch filters (Kaiser Optical Inc., Ann Arbor, MI, USA) or long-pass filters (Semrock Inc., Rochester, NY, USA) matched to these wavelengths were used to remove the laser excitation line. Laser power ranged between 20 and 30 mW. The beam was dispersed using 1200 mm^{-1} grating onto a PyLoN 400BR CCD (Princeton Instruments, Trenton, NJ, USA), cooled with liquid nitrogen to −120 °C; Winspec/32 software was used to control the CCD equipment. Sample concentrations were typically 1×10^{-5} M and spectra were obtained at 298 K. Spectra were calibrated at each excitation wavelength, using reference peaks of a 1:1 mixture of toluene and acetonitrile to within a pixel.

2.4. Quinoidal character based on harmonic oscillator model of aromaticity (HOMA)

The quinoidal character (Q) of each thiophene ring of the photosensitizers was evaluated based on the modified HOMA analysis. The Q was calculated for the ground and excited states of each photosensitizer as following Eqs. [39]:

$$Q = 1 - aromaticity \tag{1}$$

$$aromaticity = 1 - \frac{\alpha}{n}\sum_i \left[R_{\text{aromatic,i}} - R_{\text{i}}\right]^2 \tag{2}$$

$$\alpha = \left[\frac{1}{n}\sum_i \left[R_{\text{acromatic,i}} - R_{\text{quinoidal,i}}\right]^2\right]^{-1} \tag{3}$$

where Q is the quinoidal character, α is the normalization constant for the Q, n is the number of the bonds of ring of interest, $R_{\text{aromatic,i}}$ is the length of bonds i in an aromatic model, $R_{\text{quinoidal,i}}$ is the length of bonds i in a quinoidal model, and R_{i} is the bond length of the bonds i of interested molecules. For the calculation of the α constant, the aromatic and quinoidal structures of 2,6-bis(3-hexylthiophen-2-yl)dithieno[3,2-*b*:2′,3′-*d*]thiophene core unit were considered (Fig. S2), leading to the *aromaticity* being 1.0 for the aromatic core and being 0.0 for the quinoidal core. The detailed calculations are described in the Supplementary Data (Part 6).

2.5. Device fabrication

Thin photoanodes were prepared on fluorine-doped tin oxide glass (FTO, Nippon Sheet Glass Co., Ltd) by a screen-printing method. The photoanode films were composed of a 3.5 μm thick photoactive layer and a 1.5 μm thick scattering layer. These films were immersed into a 0.1 mM dye solution with 5 mM chenodeoxycholic acid as a co-adsorbent in a binary solvent of chloroform/ethanol (*v*/*v*, 7:3) for 8 h. The dye-adsorbed photoanode films were assembled with platinum (Pt) counter electrodes, sealed by a Surlyn film of 25 μm thickness (Meltonix 1170−25, Solaronix). Iodine-based electrolyte was used for devices with the following composition: 0.025 M LiI, 0.055 M I_2, 0.05 M guanidine thiocyanate (GuSCN), 0.6 M 1,2-dimethyl-3-propylimidazolium iodide, and 0.5 M 4-*tert*-butylpyridine (TBP) in a binary solvent of acetonitrile/valeronitrile (*v*/*v*, 85:15). Detailed procedure of the device fabrication is described in the Supplementary Data (Part 2).

3. Results and discussion

3.1. Molecular design and optoelectronic properties of the photosensitizers

To study the effects of the molecular structure on the CT and quinoidal properties of the photosensitizers, five photosensitizers were prepared with different bond types between the triphenylamine (TPA) donor and the DTT π-bridge, and EDGs were introduced at the *para* position of the TPA donor. These photosensitizers were labelled as follows: **S-D1** (single bond, H-), **D-D1** (double bond, H-), **T-D1** (triple bond, H-), **T-D2** (triple bond, methoxy-), and **T-D3** (triple bond, N-carbazolyl-) (Fig. 1a). Their experimental and theoretical optoelectronic properties are summarized in Table 1, including their electronic transition wavelengths, optical bandgaps, and changes in their dipole moments.

The UV−vis absorption spectra of the photosensitizers were measured to investigate their electronic transitions and light harvesting abilities. From the absorption spectra, it was apparent that all photosensitizers exhibited ICT transition bands in the range of 450−550 nm, and $\pi-\pi^*$ transition bands in the range of 360−430 nm (Fig. 2). **S-D1**, **D-D1**, and **T-D1** exhibited ICT peaks at 496, 496, and 491 nm, respectively (Table 1). In addition, among the different bond types investigated, **T-D1** exhibited the highest molar extinction coefficient (ε) for both the ICT (52,500 M^{-1} cm^{-1}) and

Table 1
Summary of photophysical and electrochemical properties of the photosensitizers.

Photosensitizer	λ_{abs}[a] [nm] (ε [M^{-1} cm^{-1}])	$E_{g,\ onset}$[b] [eV]	λ_{trans}[c] [nm]	λ_{em}[d] [nm]	$\Delta\mu$[e] [D]
S-D1	496 (44,200)	2.08	491	668	45.27
	387 (36,400)		376		
D-D1	496 (49,200)	2.04	519	650	37.48
	434 (43,300)		410		
T-D1	491 (52,500)	2.12	491	739	48.04
	388 (45,400)		389		
T-D2	487 (57,100)	2.10	494	769	60.19
	401 (50,200)		394		
T-D3	491 (39,500)	2.12	474	728	50.64
	389 (39,100)		385		

[a] λ_{abs} is the wavelength of the ICT and $\pi-\pi^*$ transition bands.
[b] $E_{g,\ onset}$ is the optical bandgaps of the photosensitizers obtained from the absorption onset.
[c] λ_{trans} is the calculated wavelength at which the ICT and $\pi-\pi^*$ electronic transitions occur.
[d] λ_{em} is the emission wavelength of the photosensitizers in 0.02 mM DCM solution.
[e] $\Delta\mu$ is the dipole moment changes in the photosensitizers at the ground and excited states.

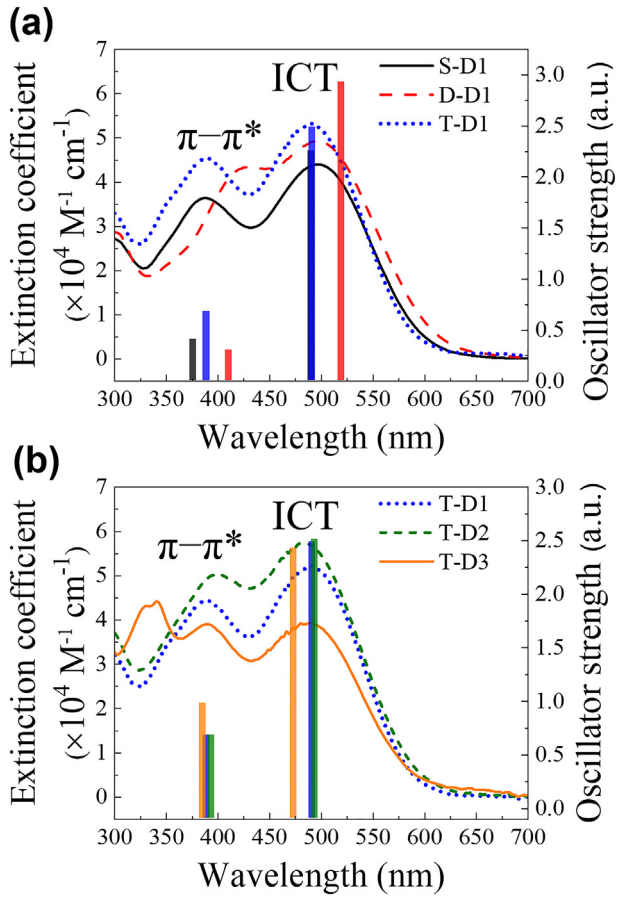

Fig. 2. Absorption spectra of the photosensitizers with different bond type (a) and EDGs (b) in 0.02 mM DCM solution. The bars are the theoretically calculated oscillator strengths of intramolecular charge transfer (ICT) and $\pi-\pi^*$ transitions using B3LYP, 6-31G(d), corresponding to the photosensitizers.

$\pi-\pi^*$ (45,400 M^{-1} cm^{-1}) transitions, followed by **D-D1** (49,200 M^{-1} cm^{-1} for the ICT transition and 43,300 M^{-1} cm^{-1} for the $\pi-\pi^*$ transition) and **S-D1** (44,200 and 36,400 M^{-1} cm^{-1}). Furthermore, the introduction of an EDG also affected the light harvesting ability, and resulted in **T-D2** exhibiting the highest molar extinction coefficient of 57,100 M^{-1} cm^{-1} for the ICT transition and 50,200 M^{-1} cm^{-1} for the $\pi-\pi^*$ transitions; this was followed by **T-D3** (39,500 M^{-1} cm^{-1} for the ICT transition and 39,100 M^{-1} cm^{-1} for the $\pi-\pi^*$ transition), which also contained an EDG. These results demonstrate that the triple bond and the EDG increase the light harvesting properties of the photosensitizers for both the ICT and $\pi-\pi^*$ transitions. The major electronic transitions, λ_{trans}, were identified using TD-DFT calculations, which were consistent with the observed UV−vis spectra (Table 1). The first electronic transitions from the highest occupied molecular orbital (HOMO) to the lowest unoccupied molecular orbital (LUMO) were found to be located between 474 and 519 nm within the ICT transition band, while the second transitions from the HOMO to the LUMO+1 were located between 376 and 410 nm within the $\pi-\pi^*$ transition band (Fig. 2, Table 1 and S2).

To understand the change in the charge density in the ground state according to the molecular modification carried out, natural bonding orbital (NBO) analysis was performed (Table S3). NBO analysis presents the group charge densities of the various fragments of the photosensitizers (*i.e.*, the donor, linker, thiophene adjacent to the donor, DTT, thiophene adjacent to the acceptor, and acceptor). A positive NBO value indicates an electron-donating ability, while a negative NBO value denotes a withdrawing ability [40]. As can be seen from Table S3, the donor and DTT fragments of the triple bond-containing **T-D1** exhibited more positive NBO values of 0.036 and 0.049 compared to those of photosensitizers bearing single (**S-D1**, 0.032 and 0.038) and double (**D-D1**, 0.025 and 0.033) bonds. These results indicated that the triple bond increased the electron-donating ability of the donor and DTT fragments. Furthermore, the methoxy-substituted donor of **T-D2** resulted in the most positive NBO value of 0.050, demonstrating that the methoxy group on the donor further enhanced the electron-donating ability of the donor. To further evaluate the charge density change attributed to photoexcitation, the dipole moment changes ($\Delta\mu$) between the ground and excited states were calculated using DFT calculations. Due to the fact that the dipole moment is expressed as the sum of the charge densities, $\Delta\mu$ indicates any change in the charge density, and correspondingly, indicates the CT properties of the photosensitizers [41]. Consistent with its molar extinction coefficient, **T-D1** exhibited a greater $\Delta\mu$ of 48.04 D compared to **S-D1** (45.27 D) and **D-D1** (37.48 D). In addition, **T-D2** exhibited the highest $\Delta\mu$ of 60.19 D upon the introduction of an EDG, while **T-D3** showed only a slightly higher $\Delta\mu$ (50.64 D) compared to **T-D1** (48.04 D). Based on these results, we confirmed that the presence of a triple bond and a methoxy group contribute to enhancing the CT properties of the photosensitizers by increasing the value of $\Delta\mu$ to the greatest extent.

3.2. Resonance Raman spectroscopy of the photosensitizers

RR spectroscopy was implemented to probe the nature of the electronic transitions of the photosensitizers. In general, the Raman intensity is enhanced when the corresponding vibrational modes imitate specific structural changes. These structural changes occur when the charge density changes for an electronic transition that is coincident with the excitation wavelength employed [42,43]. Thus, for the different electronic transitions, the contributions of the different components of the photosensitizers could be determined (Fig. 1b). Furthermore, the nuclear coordinates of the excited state, pertaining to the vibrational mode, must be displaced relative to that of the ground state for resonance Raman scattering to occur. As the magnitude of the displacement increases, the degree of resonance is enhanced [44]. Thus, the change in the nuclear coordinates between the states is a result of a change in bonding, which is related to a change in the charge density due to an electronic transition. Consequently, the relative change in this charge density can be inferred from the intensity enhancement of the RR spectra.

Thus, the RR spectra of the photosensitizers were collected with a range of excitation wavelength ranging from 375 to 515 nm, and the non-resonant FT-Raman spectra were also collected for comparison (Fig. 3b–f). It was not possible to collect the spectrum of **D-D1** at an excitation wavelength of 515 nm due to the presence of photoluminescence (PL). Similarly, in the case of **T-D3**, PL emission also precluded the excitations at 448 and 458 nm.

Two distinct enhancement profiles were observed for the RR spectra of all photosensitizers collected at excitations of 448–515 nm and at shorter wavelengths, which is consistent with the absorbance behavior of the first two electronic transitions, *i.e.*, the ICT and the $\pi-\pi^*$ transitions (Figs. 2 and 3b–3f). In the case of **T-D2**, the 448 nm excitation spectrum displays the enhancement patterns from both the ICT and $\pi-\pi^*$ transitions, consistent with the red shift of its $\pi-\pi^*$ transition (Figs. 2b and 3e). **D-D1** exhibits an even greater overlap between the ICT and $\pi-\pi^*$ transitions compared to those of the corresponding **T-D2**, with enhancement from both transitions being observed upon excitation at 458 nm (Figs. 2a and 3c).

Some prominent vibrational modes for **T-D2** are also shown in Fig. 3a, which indicate resonant Raman enhancement. These modes are localized on the triple bond (2197 cm^{-1}), the donor (1599 cm^{-1}), and the acceptor (1584 cm^{-1}). Other key vibrational modes are described in Tables S4–S8. At high energy excitations (375–413 nm), the bands originating from the triple bond and the donor show greater enhancements than the acceptor band. In contrast, at low energy excitations (448–515 nm), the acceptor-based modes exhibit higher intensities. Two-dimensional contour maps of the Raman intensity (1550–1650 cm^{-1}) show how the relative intensity of the noted donor (~1600 cm^{-1}) and acceptor (~1584 cm^{-1}) modes change with the excitation wavelength

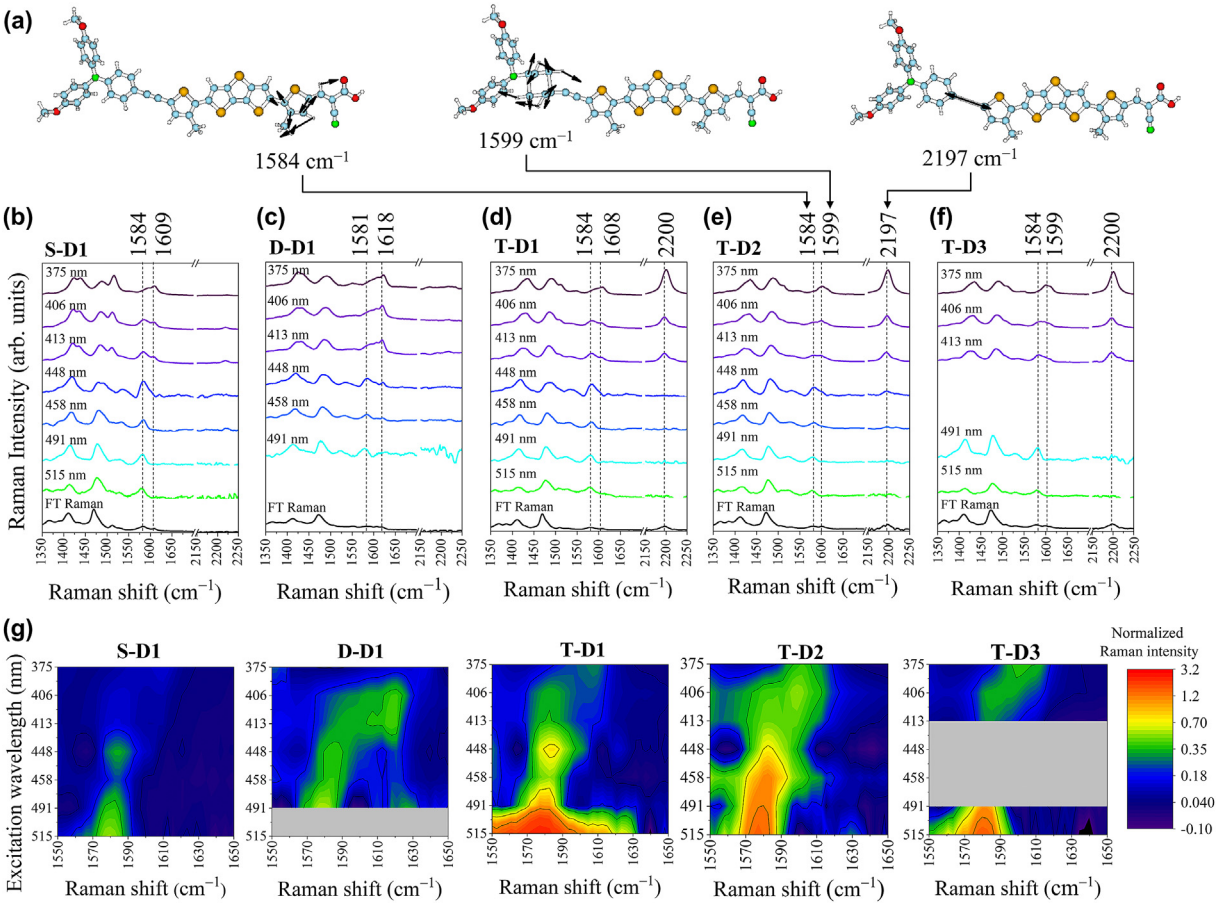

Fig. 3. (a) Vibration modes of **T-D2** which are assigned to vibration of the acceptor, the donor, and the triple bond at 1584, 1599, and 2197 cm^{-1}, respectively. (b–f) RR spectra of the photosensitizers in DCM solutions. Non-resonant FT-Raman spectra are given at the bottom as reference spectra. From bottom to top, the excitation wavelengths get shorter from 515 to 375 nm. The Raman shifts (cm^{-1}) of the vibration modes for the acceptor, the donor, and the triple bond are presented at the top of the RR spectrum for each photosensitizer. (g) Two-dimensional contour maps of the Raman intensity in the range from 1550 to 1650 cm^{-1} in the RR spectra normalized to the Raman intensity of the band at 702 cm^{-1} corresponding to DCM. The Raman intensities were mapped along the wavenumber depending on the excitation wavelength.

(Fig. 3g). This indicates that the low energy excitations (448–515 nm) exhibit notable CT to the acceptor, while the high energy excitations (375–413 nm) have more π–π^* transition character centered on the donor and the DTT core. This is consistent with the DFT calculation results (Fig. S1 and Table S2). In addition, comparing the vibrational modes common to all the photosensitizers to that of the solvent band, it was shown that **T-D1** exhibited a greater intensity for the acceptor mode (1584 cm^{-1}) compared to the cases of **S-D1** and **D-D1**, which resulted from a greater change in the charge density caused by the triple bond. Furthermore, **T-D2**, which possesses a triple bond and a methoxy group, showed the greatest resonance enhancement for the donor, indicating that the incorporation of these structural features enhanced the CT properties.

3.3. Quinoidal properties of the photosensitizers

Upon photoexcitation, a change in the electronic structure from an aromatic to a quinoidal structure can drive the CT process by generating a diradicaloid, which consequently enhances the CT properties (Fig. 4) [45,46]. Thus, the quinoidal properties of the photosensitizers containing different bond types and EDGs were investigated using two geometric indices of aromaticity; the *Q* based on a HOMA and bond length analyses (Table 2 and Figs. 4 and 5) [39,46,47]. The *Q* at the ground (S_0) and first excited (S_1) states of the thiophene rings assigned to a–c were obtained using Eqs. (1)–(3), and their values are summarized in Table 2 and S10.

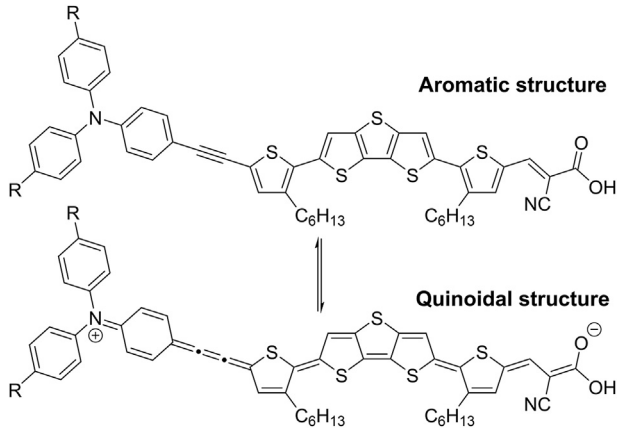

Fig. 4. Aromatic and quinoidal structures of the photosensitizers examined.

As indicated in Table 2, all thiophene rings of the π-bridges exhibited an increase in their *Q* after transition from the S_0 to the S_1 state, corresponding to the ICT transition. This result indicates that the photosensitizers possess increased quinoidal properties in the excited state. In particular, **T-D1** showed greater changes in *Q* (ΔQ) for the individual thiophene rings "a–c" and higher averaged ΔQ values than **S-D1** and **D-D1**, indicating that the triple bond is more effective in promoting the quinoidal properties than single and double bonds. Therefore, the strong quinoidal properties in the S_1 state of **T-D1** relative to the S_0 state contributes to the strongest CT properties. The introduction of EDGs was also found to further affect the *Q*. More specifically, **T-D3** exhibited a more significant ΔQ for thiophene rings "a–c" than the corresponding **T-D1**. However, **T-D2** exhibited the greatest ΔQ only at thiophene ring "c", which was adjacent to the acceptor. This result demonstrates that **T-D2**, which bears the strongest EDG, exhibited quinoidal properties adjacent to the acceptor and the donor groups, which corresponds to the RR spectroscopic result discussed above (Fig. 3). Based on the ΔQ analysis, it became apparent that the presence of a triple bond and an EDG can enhance the quinoidal property of an aromatic photosensitizer after photoexcitation, resulting in CT enhancement. Moreover, HOMA analysis confirmed this observation (Table S9). Such ΔQ analysis could be applicable to other series of photosensitizers containing an identical core unit (*e.g.,* zinc-porphyrin), as demonstrated in the Supplementary Data (Part 7).

In addition, the bond lengths between the S_0 and S_1 states were also compared to analyze the degree of the quinoidal property at the S_1 state (Fig. 5b and c, representing the bond lengths of the π-bridge and the donor, respectively). All photosensitizers exhibited alternative changes in their bond lengths, which is a typical phenomenon when the quinoidal structure exists [46,48–51]. Among the various photosensitizers with different bond types, **T-D1** exhibited the largest changes in the π-bridge bond length, followed by **S-D1** and **D-D1** (Fig. 5b), which is consistent with the RR spectroscopic results and the ΔQ analyses described above. For the photosensitizers bearing different EDGs (Fig. 5c), **T-D2** exhibited the largest changes in bond length on the TPA donor, followed by **T-D3** and **T-D1**, which is again consistent with the RR spectroscopic results and the ΔQ analyses (Fig. 3g and Table 2). Based on these results, we confirmed the effect of the triple bond and the EDG on the enhancement of the quinoidal properties.

Table 2
Changes in quinoidal characters (ΔQ) between S_0 and S_1 states of the photosensitizers, corresponding to the ICT transition.

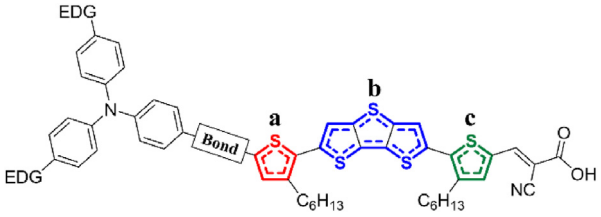

Photosensitizer	ΔQ (%)[a]			Averaged ΔQ (%)[b]
	a	b	c	
S-D1	13.2	11.0	11.2	11.8
D-D1	14.5	9.8	10.3	11.5
T-D1	16.2	15.5	12.5	14.7
T-D2	6.8	9.1	13.4	9.8
T-D3	16.1	20.3	15.3	17.2

[a] ΔQ (%) = (Quinoidal character at S_1 − Quinoidal character at S_0) × 100.
[b] Averaged ΔQ (%) is average of ΔQ for a, b, and c rings.

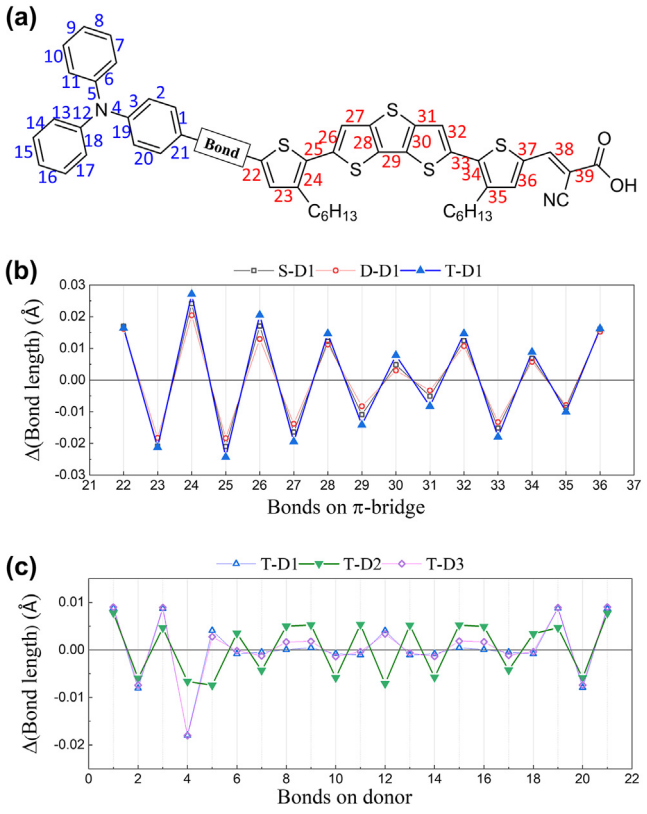

Fig. 5. (a) Numbering order of bonds, and (b, c) bond length changes of the photosensitizers by the photoexcitation. The bond length changes of the π-bridge are shown for **S-D1**, **D-D1**, and **T-D1** (b). For **T-D1**, **T-D2**, and **T-D3**, the bond length changes of the donor are shown (c).

3.4. Photovoltaic performances of the DSSCs

The photovoltaic performances of the five photosensitizers in the DSSCs were then evaluated to confirm their CT and quinoidal properties. More specifically, the five photosensitizers were applied to DSSCs containing thin photoanode films (3.5 μm) and an iodine electrolyte. Table 3 shows the obtained results for the various devices in terms of the short-circuit photocurrent density (J_{SC}), the open-circuit voltage (V_{OC}), the fill factor (FF), and the PCE (η). Fig. 6 presents the current density–voltage (J–V) curves of the devices under 1 sun illumination (AM 1.5G). As indicated, the PCE and J_{SC} values of the photosensitizers were largely affected by the CT properties of the photosensitizers. Among the photosensitizers studied, **T-D2** exhibited the highest PCE (η = 7.6%) and J_{SC} (13.2 mA cm^{-2}), followed by **T-D3** (η = 7.1%, J_{SC} = 12.3 mA cm^{-2}), **T-D1** (η = 6.3%, J_{SC} = 13.7 mA cm^{-2}), **S-D1** (η = 6.4%, J_{SC} = 12.3 mA cm^{-2}), and **D-D1** (η = 5.6%, J_{SC} = 10.6 mA cm^{-2}). Thus, the higher J_{SC} of **T-D1** compared to those of **S-D1** and **D-D1** confirms the superior CT properties achieved upon introduction of the triple bond into the structure. In addition, **T-D2** gave a higher PCE than **T-D1**, thereby providing further evidence for the previously reported electron-donating effect of the methoxy group [18]. Furthermore, **T-D2** exhibited the highest V_{OC} among the photosensitizers, and this was attributed to the fact that enhancement of the dipole moment by the methoxy group induces an upward shift of the TiO_2 conduction band [18,52,53]. Overall, **T-D2** exhibited the best performance among the various materials studied, thereby confirming that the introduction of the triple bond and the presence of the methoxy groups on the *para* position of the donor can improve the J_{SC} and PCE of the DSSCs by enhancing the CT properties of the photosensitizer.

Table 3
Photovoltaic parameters of DSSCs in iodine electrolyte under AM 1.5G.

Photosensitizers	η [%]	J_{SC} [mA cm^{-2}]	V_{OC} [V]	FF
S-D1	6.4	12.3	0.73	0.72
D-D1	5.6	10.6	0.71	0.75
T-D1	6.3	13.7	0.70	0.66
T-D2	7.6	13.2	0.77	0.75
T-D3	7.1	12.3	0.76	0.76

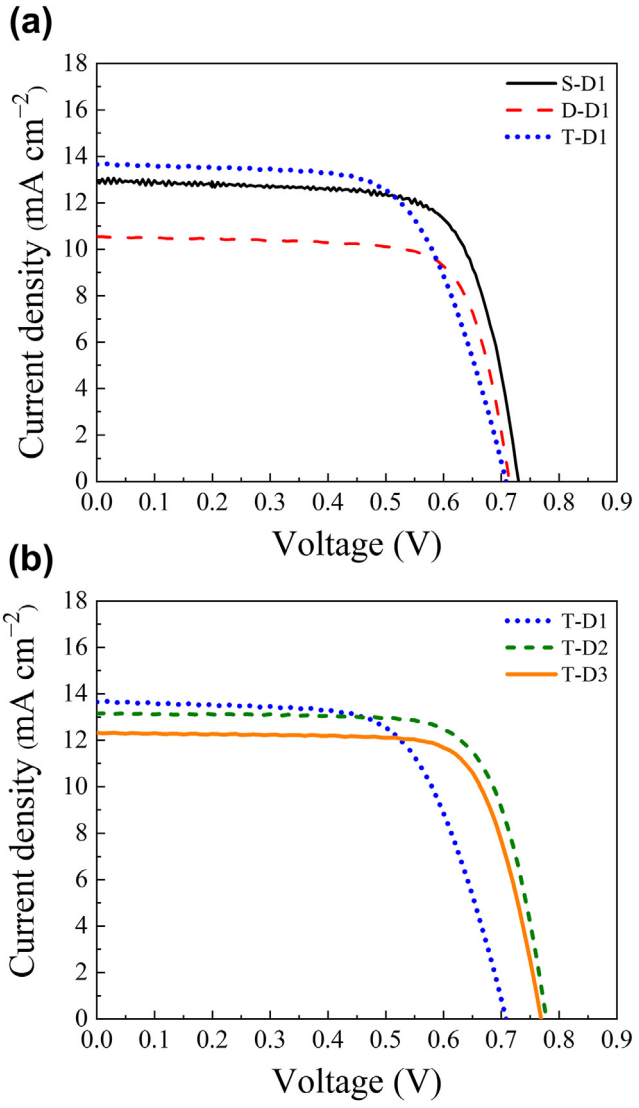

Fig. 6. (a) J–V curves of the photosensitizers with different bond types; **S-D1**, **D-D1**, and **T-D1**. (b) J–V curves of the photosensitizers with different EDGs; **T-D1**, **T-D2**, and **T-D3**.

4. Conclusions

Five donor–π-bridge–acceptor (D–π–A)-structured photosensitizers containing different bond types and electron donating groups (EDGs) on the donor were investigated to explore their charge transfer (CT) properties. For this purpose, resonance Raman (RR) spectroscopy and density functional theory calculations were

employed. The RR spectra revealed that the presence of a triple bond and an EDG enhanced the CT properties of the photosensitizers in terms of the intramolecular charge transfer and $\pi-\pi^*$ transitions. A quinoidal character based on a harmonic oscillator model of aromaticity and bond length analyses demonstrated that the triple bond effectively induced the quinoidal property to greater extent than single and double bonds, while EDGs enhanced the quinoidal property, especially for the thiophene spacer adjacent to the acceptor, resulting in improved CT properties. Upon the application of these photosensitizers to dye-sensitized solar cells (DSSCs), **T-D2**, which contains a triple bond and a strong EDG, exhibited the highest power conversion efficiency of 7.6%, owing to the enhanced CT and quinoidal properties. We therefore confirmed that the CT and quinoidal properties are enhanced by the introduction of a triple bond and an EDG, thereby elucidating the relationship between the molecular structure and the CT properties. This research is expected to contribute to establishing molecular design strategies to obtain photosensitizers with superior CT properties, which will result in breakthrough DSSC performances.

Author contributions

Wang-Hyo Kim contributed to Conceptualization, Formal analysis, Investigation, Writing – original draft, Writing – review & editing, and Visualization. Joseph I. Mapley contributed to Conceptualization, Formal analysis, Investigation, Writing – original draft, Writing – review & editing, and Visualization. Deok-Ho Roh contributed to Formal analysis, Investigation, Writing – original draft, Writing – review & editing, and Visualization. Jeong Soo Kim contributed to Resources. So Yeon Yoon contributed to Formal analysis and Investigation. Keith C. Gordon contributed to Conceptualization, Writing – review & editing, Supervision, and Project administration. Tae-Hyuk Kwon contributed to Conceptualization, Writing – original draft, Writing – review & editing, Supervision, Project administration, and Funding acquisition.

Data availability

The raw/processed data required to reproduce these findings cannot be shared at this time due to technical or time limitations. Data will be made available on request.

Declaration of competing interest

The authors declare that they have no known competing financial interests or personal relationships that could have appeared to influence the work reported in this paper.

Acknowledgement

The authors gratefully acknowledge the financial support provided by the National Research Foundation of Korea funded by the Ministry of Science, ICT and Future Planning (2020R1C1C1014936), and the 2020 Fundamental Research Development Project funded by Korea Electric Power Corporation (KEPCO) (R20XO02-3).

Appendix A. Supplementary data

Supplementary data to this article can be found online at https://doi.org/10.1016/j.mtadv.2021.100180.

References

[1] M.B. Desta, N.S. Vinh, C.H. Pavan Kumar, S. Chaurasia, W.-T. Wu, J.T. Lin, T.-C. Wei, E. Wei-Guang Diau, Pyrazine-incorporating panchromatic sensitizers for dye sensitized solar cells under one sun and dim light, J. Mater. Chem. A 6 (2018) 13778–13789, https://doi.org/10.1039/C8TA04774J.

[2] I.P. Liu, W.-H. Lin, C.-M. Tseng-Shan, Y.-L. Lee, Importance of compact blocking layers to the performance of dye-sensitized solar cells under ambient light conditions, ACS Appl. Mater. Interfaces 10 (2018) 38900–38905, https://doi.org/10.1021/acsami.8b13181.

[3] M. Freitag, J. Teuscher, Y. Saygili, X. Zhang, F. Giordano, P. Liska, J. Hua, S.M. Zakeeruddin, J.-E. Moser, M. Grätzel, A. Hagfeldt, Dye-sensitized solar cells for efficient power generation under ambient lighting, Nat. Photonics 11 (2017) 372–378, https://doi.org/10.1038/nphoton.2017.60.

[4] A. Hagfeldt, G. Boschloo, L. Sun, L. Kloo, H. Pettersson, Dye-sensitized solar cells, Chem. Rev. 110 (2010) 6595–6663, https://doi.org/10.1021/cr900356p.

[5] B.-M. Kim, M.-H. Lee, V.S. Dilimon, J.S. Kim, J.S. Nam, Y.-G. Cho, H.K. Noh, D.-H. Roh, T.-H. Kwon, H.-K. Song, Indoor-light-energy-harvesting dye-sensitized photo-rechargeable battery, Energy Environ. Sci. 13 (2020) 1473–1480, https://doi.org/10.1039/C9EE03245B.

[6] S. Venkatesan, I.P. Liu, C.-W. Li, C.-M. Tseng-Shan, Y.-L. Lee, Quasi-solid-state dye-sensitized solar cells for efficient and stable power generation under room light conditions, ACS Sustain. Chem. Eng. 7 (2019) 7403–7411, https://doi.org/10.1021/acssuschemeng.9b00754.

[7] K. Fan, J. Yu, W. Ho, Improving photoanodes to obtain highly efficient dye-sensitized solar cells: a brief review, Mater. Horiz. 4 (2017) 319–344, https://doi.org/10.1039/C6MH00511J.

[8] J.H. Park, D.G. Nam, B.M. Kim, M.Y. Jin, D.H. Roh, H.S. Jung, D.H. Ryu, T.H. Kwon, Planar D-D-π-A organic sensitizers for thin-film photoanodes, ACS Energy Lett 2 (2017) 1810–1817, https://doi.org/10.1021/acsenergylett.7b00438.

[9] N. Shahzad, F. Risplendi, D. Pugliese, S. Bianco, A. Sacco, A. Lamberti, R. Gazia, E. Tresso, G. Cicero, Comparison of hemi-squaraine sensitized TiO_2 and ZnO photoanodes for DSSC applications, J. Phys. Chem. C 117 (2013) 22778–22783, https://doi.org/10.1021/jp406824f.

[10] D.-H. Roh, K.M. Kim, J.S. Nam, U.-Y. Kim, B.-M. Kim, J.S. Kim, T.-H. Kwon, Strategy for improved photoconversion efficiency in thin photoelectrode films by controlling π-spacer dihedral angle, J. Phys. Chem. C 120 (2016) 24655–24666, https://doi.org/10.1021/acs.jpcc.6b08262.

[11] A. Carella, F. Borbone, R. Centore, Research progress on photosensitizers for DSSC, Front. Chem. 6 (2018) 481, https://doi.org/10.3389/fchem.2018.00481.

[12] Y. Wu, W. Zhu, Organic sensitizers from D–π–A to D–A–π–A: effect of the internal electron-withdrawing units on molecular absorption, energy levels and photovoltaic performances, Chem. Soc. Rev. 42 (2013) 2039–2058, https://doi.org/10.1039/C2CS35346F.

[13] A. Yella, H.-W. Lee, H.N. Tsao, C. Yi, A.K. Chandiran, M.K. Nazeeruddin, E.W.-G. Diau, C.-Y. Yeh, S.M. Zakeeruddin, M. Grätzel, Porphyrin-sensitized solar cells with cobalt (II/III)–Based redox electrolyte exceed 12 percent efficiency, Science 334 (2011) 629–634, https://doi.org/10.1126/science.1209688.

[14] S. Mathew, A. Yella, P. Gao, R. Humphry-Baker, B.F.E. Curchod, N. Ashari-Astani, I. Tavernelli, U. Rothlisberger, M.K. Nazeeruddin, M. Grätzel, Dye-sensitized solar cells with 13% efficiency achieved through the molecular engineering of porphyrin sensitizers, Nat. Chem. 6 (2014) 242–247, https://doi.org/10.1038/nchem.1861.

[15] K. Susumu, T.V. Duncan, M.J. Therien, Potentiometric, electronic structural, and ground- and excited-state optical properties of conjugated bis[(porphinato)zinc(II)] compounds featuring proquinoidal spacer units, J. Am. Chem. Soc. 127 (2005) 5186–5195, https://doi.org/10.1021/ja040243h.

[16] J.M. Woods, J.P. Pennington, J.F. Stobaugh, The derivatization of proquinoidal analytes with 1,2-Diphenylethane-1,2-diamine (DPE) and benzylamine (BA): an investigation of products, yields, kinetics and reagent selectivity, Chromatographia 78 (2015) 163–178, https://doi.org/10.1007/s10337-014-2828-0.

[17] J.S. Kim, B.-M. Kim, U.-Y. Kim, H. Shin, J.S. Nam, D.-H. Roh, J.-H. Park, T.-H. Kwon, Molecular engineering for enhanced charge transfer in thin-film photoanode, ACS Appl. Mater. Interfaces 9 (2017) 34812–34820, https://doi.org/10.1021/acsami.7b08098.

[18] J.-H. Park, U.-Y. Kim, B.-M. Kim, W.-H. Kim, D.-H. Roh, J.S. Kim, T.-H. Kwon, Molecular design strategy toward robust organic dyes in thin-film photoanodes, ACS Appl. Energy Mater. 2 (2019) 4674–4682, https://doi.org/10.1021/acsaem.8b02100.

[19] M. Planells, L. Pellejà, J.N. Clifford, M. Pastore, F. De Angelis, N. López, S.R. Marder, E. Palomares, Energy levels, charge injection, charge recombination and dye regeneration dynamics for donor–acceptor π-conjugated organic dyes in mesoscopic TiO2 sensitized solar cells, Energy Environ. Sci. 4 (2011) 1820–1829, https://doi.org/10.1039/C1EE01060C.

[20] Y. Liu, X. Zhang, C. Li, Y. Tian, F. Zhang, Y. Wang, W. Wu, B. Liu, Energy-level control via molecular planarization and its effect on interfacial charge-transfer processes in dye-sensitized solar cells, J. Phys. Chem. C 123 (2019) 13531–13537, https://doi.org/10.1021/acs.jpcc.9b03986.

[21] L. Tian, Y. Wang, Y. Zhang, X. Li, W. Wu, B. Liu, Molecular engineering of indoline dyes and their application in dye-sensitized solar cells: effect of planarity and side chain on interfacial charge-transfer processes, ACS Appl. Energy Mater. 4 (2021) 242−248, https://doi.org/10.1021/acsaem.0c02199.
[22] K.R. Siefermann, C.D. Pemmaraju, S. Neppl, A. Shavorskiy, A.A. Cordones, J. Vura-Weis, D.S. Slaughter, F.P. Sturm, F. Weise, H. Bluhm, M.L. Strader, H. Cho, M.-F. Lin, C. Bacellar, C. Khurmi, J. Guo, G. Coslovich, J.S. Robinson, R.A. Kaindl, R.W. Schoenlein, A. Belkacem, D.M. Neumark, S.R. Leone, D. Nordlund, H. Ogasawara, O. Krupin, J.J. Turner, W.F. Schlotter, M.R. Holmes, M. Messerschmidt, M.P. Minitti, S. Gul, J.Z. Zhang, N. Huse, D. Prendergast, O. Gessner, Atomic-scale perspective of ultrafast charge transfer at a dye−semiconductor interface, J. Phys. Chem. Lett. 5 (2014) 2753−2759, https://doi.org/10.1021/jz501264x.
[23] S. Chen, L. Yang, J. Zhang, Y. Yuan, X. Dong, P. Wang, Excited-state and charge carrier dynamics in a high-photovoltage and thermostable dye-sensitized solar cell, ACS Photonics 4 (2017) 165−173, https://doi.org/10.1021/acsphotonics.6b00772.
[24] Y. Tang, Y. Wang, X. Li, H. Ågren, W.-H. Zhu, Y. Xie, Porphyrins containing a triphenylamine donor and up to eight alkoxy chains for dye-sensitized solar cells: a high efficiency of 10.9, ACS Appl. Mater. Interfaces 7 (2015) 27976−27985, https://doi.org/10.1021/acsami.5b10624.
[25] C. Yan, W. Ma, Y. Ren, M. Zhang, P. Wang, Efficient triarylamine−perylene dye-sensitized solar cells: influence of triple-bond insertion on charge recombination, ACS Appl. Mater. Interfaces 7 (2015) 801−809, https://doi.org/10.1021/am507261j.
[26] M. Wächtler, J. Guthmuller, L. González, B. Dietzek, Analysis and characterization of coordination compounds by resonance Raman spectroscopy, Coord. Chem. Rev. 256 (2012) 1479−1508, https://doi.org/10.1016/j.ccr.2012.02.004.
[27] R. Petry, M. Schmitt, J. Popp, Raman spectroscopy—a prospective tool in the life sciences, ChemPhysChem 4 (2003) 14−30, https://doi.org/10.1002/cphc.200390004.
[28] W.R. Browne, N.M. O'Boyle, J.J. McGarvey, J.G. Vos, Elucidating excited state electronic structure and intercomponent interactions in multicomponent and supramolecular systems, Chem. Soc. Rev. 34 (2005) 641−663, https://doi.org/10.1039/B400513A.
[29] R. Horvath, K.C. Gordon, Understanding excited-state structure in metal polypyridyl complexes using resonance Raman excitation profiles, time-resolved resonance Raman spectroscopy and density functional theory, Coord. Chem. Rev. 254 (2010) 2505−2518, https://doi.org/10.1016/j.ccr.2009.11.015.
[30] T.-H. Kwon, V. Armel, A. Nattestad, D.R. MacFarlane, U. Bach, S.J. Lind, K.C. Gordon, W. Tang, D.J. Jones, A.B. Holmes, Dithienothiophene (DTT)-Based dyes for dye-sensitized solar cells: synthesis of 2,6-dibromo-DTT, J. Org. Chem. 76 (2011) 4088−4093, https://doi.org/10.1021/jo2001484.
[31] A.D. Becke, Density-functional thermochemistry. III.The role of exact exchange, J. Chem. Phys. 98 (1993) 5648−5652, https://doi.org/10.1063/1.464913.
[32] P.J. Stephens, F.J. Devlin, C.F. Chabalowski, M.J. Frisch, Ab initio calculation of vibrational absorption and circular dichroism spectra using density functional force fields, J. Phys. Chem. 98 (1994) 11623−11627, https://doi.org/10.1021/j100096a001.
[33] T. Yanai, D.P. Tew, N.C. Handy, A new hybrid exchange-correlation functional using the Coulomb-attenuating method (CAM-B3LYP), Chem. Phys. Lett. 393 (2004) 51−57, https://doi.org/10.1016/j.cplett.2004.06.011.
[34] J. Tomasi, B. Mennucci, R. Cammi, Quantum mechanical continuum solvation models, Chem. Rev. 105 (2005) 2999−3094, https://doi.org/10.1021/cr9904009.
[35] M. J. Frisch, G. W. Trucks, H. B. Schlegel, G. E. Scuseria, M. A. Robb, J. R. Cheeseman, G. Scalmani, V. Barone, B. Mennucci, G. A. Petersson, H. Nakatsuji, M. Caricato, X. Li, H. P. Hratchian, A. F. Izmaylov, J. Bloino, G. Zheng, J. L. Sonnenberg, M. Hada, M. Ehara, K. Toyota, R. Fukuda, J. Hasegawa, M. Ishida, T. Nakajima, Y. Honda, O. Kitao, H. Nakai, T. Vreven, J. A. Montgomery, J. E. Peralta, F. Ogliaro, M. Bearpark, J. J. Heyd, E. Brothers, K. N. Kudin, V. N. Staroverov, R. Kobayashi, J. Norm, K. Raghavachari, A. Rendell, J. C. Burant, S. S. Iyengar, J. Tomasi, M. Cossi, N. Rega, J. M. Millam, M. Klene, J. E. Knox, J. B. Cross, V. Bakken, C. Adamo, J. Jaramillo, R. Gomperts, R. E. Stratmann, O. Yazyev, A. J. Austin, R. Cammi, C. Pomelli, J. W. Ochterski, R. L. Martin, K. Morokuma, V. G. Zakrzewski, G. A. Voth, P. Salvador, J. J. Dannenberg, S. Dapprich, A. D. Daniels, Ö. Farkas, J. B. Foresman, J. V. Ortiz, J. Cioslowski, D. J. Fox, Gaussian 09 Revision D.01, 2013. (Wallingford, CT).
[36] A.P. Scott, L. Radom, Harmonic vibrational frequencies:an evaluation of Hartree−Fock ,Møller−Plesset ,quadratic configuration interaction ,density functional theory ,and semiempirical scale factors, J. Phys. Chem. 100 (1996) 16502−16513, https://doi.org/10.1021/jp960976r.
[37] G. Schaftenaar, J.H. Noordik, Molden: a pre- and post-processing program for molecular and electronic structures, J. Comput. Aided Mol. Des. 14 (2000) 123−134, https://doi.org/10.1023/a:1008193805436.
[38] J.E. Barnsley, G.E. Shillito, J.I. Mapley, C.B. Larsen, N.T. Lucas, K.C. Gordon, Walking the emission tightrope: spectral and computational analysis of some dual-emitting benzothiadiazole donor-acceptor dyes, J. Phys. Chem. A 122 (2018) 7991−8006, https://doi.org/10.1021/acs.jpca.8b05361.
[39] K. Klaue, W. Han, P. Liesfeld, F. Berger, Y. Garmshausen, S. Hecht, Donor−acceptor dihydropyrenes switchable with near-infrared light, J. Am. Chem. Soc. 142 (2020) 11857−11864, https://doi.org/10.1021/jacs.0c04219.
[40] S. Mandal, G.R. Kandregula, K. Ramanujam, Replacing aromatic π-system with cycloalkyl in triphenylamine dyes to impact intramolecular charge transfer in dyes pertaining to dye-sensitized solar cells application, J. Photochem. Photobiol., A 403 (2020) 112862, https://doi.org/10.1016/j.jphotochem.2020.112862.
[41] J.F. Harrison, Relationship between the charge distribution and dipole moment functions of CO and the related molecules CS, SiO, and SiS, J. Phys. Chem. A 110 (2006) 10848−10857, https://doi.org/10.1021/jp058279z.
[42] R.J.H. Clark, T.J. Dines, Resonance Raman spectroscopy, and its application to inorganic Chemistry, Angew. Chem. Int. Ed. 25 (1986) 131−158, https://doi.org/10.1002/anie.198601311.
[43] A.Y. Hirakawa, M. Tsuboi, Molecular geometry in an excited electronic state and a preresonance Raman effect, Science 188 (1975) 359−361, https://doi.org/10.1126/science.188.4186.359.
[44] J.I. Zink, L. Tutt, Y.Y. Yang, Excited state distortions determined by electronic and Raman spectroscopy, in: Excited States and Reactive Intermediates, vol. 307, American Chemical Society, 1986, pp. 39−56.
[45] P.M. Burrezo, W.D. Zeng, M. Moos, M. Holzapfel, S. Canola, F. Negri, C. Rovira, J. Veciana, H. Phan, J.S. Wu, C. Lambert, J. Casado, Perylene π-bridges equally delocalize anions and cations: proportioned quinoidal and aromatic content, Angew. Chem. Int. Ed. 58 (2019) 14467−14471, https://doi.org/10.1002/anie.201905657.
[46] J. Kim, J. Oh, S. Park, J.L. Zafra, J.R. DeFrancisco, D. Casanova, M. Lim, J.D. Tovar, J. Casado, D. Kim, Two-electron transfer stabilized by excited-state aromatization, Nat. Commun. 10 (2019) 4983, https://doi.org/10.1038/s41467-019-12986-w.
[47] T.M. Krygowski, H. Szatylowicz, O.A. Stasyuk, J. Dominikowska, M. Palusiak, Aromaticity from the viewpoint of molecular geometry: application to planar systems, Chem. Rev. 114 (2014) 6383−6422, https://doi.org/10.1021/cr400252h.
[48] E.V. Canesi, D. Fazzi, L. Colella, C. Bertarelli, C. Castiglioni, Tuning the quinoid versus biradicaloid character of thiophene-based heteroquaterphenoquinones by means of functional groups, J. Am. Chem. Soc. 134 (2012) 19070−19083, https://doi.org/10.1021/ja3072385.
[49] K. Kawabata, M. Saito, I. Osaka, K. Takimiya, Very small bandgap π-conjugated polymers with extended thienoquinoids, J. Am. Chem. Soc. 138 (2016) 7725−7732, https://doi.org/10.1021/jacs.6b03688.
[50] S.N. Intorp, M. Hodecker, M. Müller, O. Tverskoy, M. Rosenkranz, E. Dmitrieva, A.A. Popov, F. Rominger, J. Freudenberg, A. Dreuw, U.H.F. Bunz, Quinoidal azaacenes: 99%Diradical character, Angew. Chem. Int. Ed. 59 (2020) 12396−12401, https://doi.org/10.1002/anie.201915977.
[51] S. Ray, S. Sharma, U. Salzner, S. Patil, Synthesis and characterization of quinoidal diketopyrrolopyrrole derivatives with exceptionally high electron affinities, J. Phys. Chem. C 121 (2017) 16088−16097, https://doi.org/10.1021/acs.jpcc.7b04085.
[52] E. Ronca, M. Pastore, L. Belpassi, F. Tarantelli, F. De Angelis, Influence of the dye molecular structure on the TiO_2 conduction band in dye-sensitized solar cells: disentangling charge transfer and electrostatic effects, Energy Environ. Sci. 6 (2013) 183−193, https://doi.org/10.1039/C2EE23170K.
[53] B. Liu, B. Wang, R. Wang, L. Gao, S. Huo, Q. Liu, X. Li, W. Zhu, Influence of conjugated π-linker in D−D−π−A indoline dyes: towards long-term stable and efficient dye-sensitized solar cells with high photovoltage, J. Mater. Chem. A 2 (2014) 804−812, https://doi.org/10.1039/C3TA13993J.